Smart Structures and Systems, Vol. 4, No. 1 (2008) 85-98

DOI: http://dx.doi.org/10.12989/sss.2008.4.1.085

Design of an actuator for simulating wind-induced response of a building structure

Eun Churn Park, Sang-Hyun Lee†, Kyung-Won Min, Lan Chung, Sung-Kyung Lee and Seung-Ho Cho

Department of Architectural Engineering, Dankook University, Jukjeon-dong, San 44-1, Suji-Gu, Yongin-si, Gyeonggi-do, Korea

Eunjong Yu

Department of Architectural Engineering, Hanyang University, 17, Haengdang-dong, Seongdong-gu, Seoul, Korea

Kyung-Soo Kang

Department of Architectural Engineering, Tongmyong University, Pusan, Korea

(Received October 30, 2006, Accepted August 9, 2007)

Abstract. In this paper, excitation systems using a linear mass shaker (LMS) and an active tuned mass damper (ATMD) are presented to simulate the wind induced responses of a building structure. The actuator force for the excitation systems is calculated by using the inverse transfer function of a target structural response to the actuator. Filter and envelop functions are used to prevent the actuator from exciting unexpected modal responses and an initial transient response and thus, to minimize the error between the wind and actuator induced responses. The analyses results from a 76-story benchmark building problem for which the wind load obtained by a wind tunnel test is given, indicate that the excitation system installed at a specific floor can approximately reproduce the structural responses induced by the wind load applied to each floor of the structure. The excitation system designed by the proposed method can be effectively used for evaluating the wind response characteristics of a practical building structure and for obtaining an accurate analytical model of the building under wind load.

Keywords: actuator; linear mass shaker; active tuned mass damper; wind-induced response.

1. Introduction

The dynamic response characteristics of a building structure excited by input signals such as a real earthquake or wind load need to be identified accurately not only for the evaluation of the safety and serviceability of the building structure, but for the verification of the analytical model used in the seismic or wind design (Ljung 1987). In the field of system identification (SI), which constructs system matrices describing accurate input/output relationships, the input must have enough energy to excite the

†Corresponding Author, E-mail: lshyun00@dankook.ac.kr

fundamental structural modes, and a good quality of the output containing structural information should be measured (Alvin & Park 1994 and Madenci & Barut 1994)).

Dyke, *et al*. (1994) obtained controller canonical form state space realization for a small scale, three story building by using both an active mass driver and shaking table and measuring the absolute floor acceleration. Juang(1994) proposed the observer/Kalman filter identification using system Markov parameters in time-domain. These studies presented the mathematical models that accurately describe input/output relationships but did not provide physical mass, stiffness, and damping matrices. To tackle this problem, a finite element model based SI techniques are developed in the field of health monitoring or damage detection. Herman and Bart (2003), Yu, *et al*. (2005) performed a series of ambient vibration measurement and force vibration tests on a four-story reinforced concrete building by using linear and eccentric mass shakers, and updated the analytical finite element (FE) model based on the collected dynamic data. Also, Yu, *et al.* (2005) presented a linear shaker system to simulate a linear elastic structural seismic response. However, it is practically difficult to excite large scale civil structures to show inelastic response by using artificial mass-type actuator in spite of the fact that inelastic structural response should be considered in seismic design.

In the field of wind engineering, because it is impossible to measure the real wind load applied to each floor of a structure, the relationship between the structural responses and the wind load is difficult to obtain. Accordingly, SI of a building structure excited by wind load is generally performed only using the output data obtained by ambient vibration measurements without information on the input. Such output based SI using natural excitation has problems in that the measurement equipment has to be operated at all times during the experiment and the quality of the measured output is not good enough to use for accurate evaluation of the dynamic characteristics of a structure because the energy of natural excitation is generally insufficient to excite a structure to the degree of vibration considered in design.

In this paper, a linear mass shaker (LMS) and active tuned mass damper (ATMD) which are used for simulating the wind-induced responses of a building structure are presented, as shown in Fig. 1. For the linear actuator to keep the structure in the target response trajectory, an inverse transfer function of a

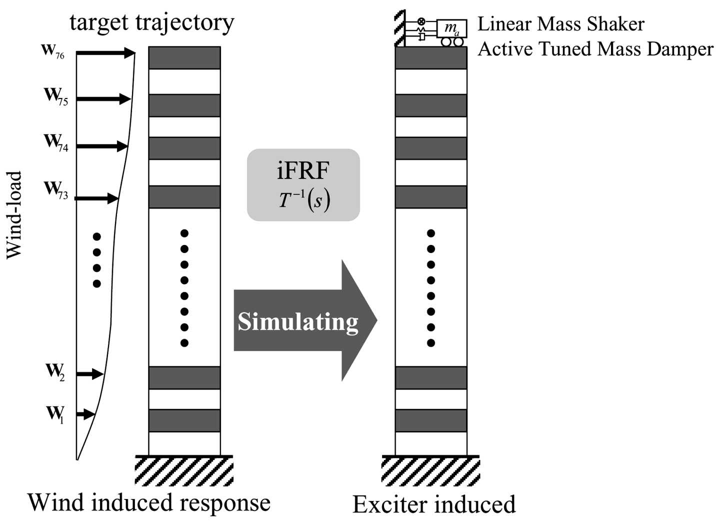

Fig. 1 Scheme of simulation of wind induced responses using LMS and ATMD

structural response to the shaker force is obtained by using a state space form governing equation of the structure, and a discrete Fourier transform of a structural response is performed. Filter and an envelop function are used to prevent the shaker from exciting unexpected modal responses and initial transient responses and thus, to minimize the error between wind- and actuator-induced responses. The effectiveness of the proposed method is verified through a numerical example of a 76 story-benchmark building excited by wind load whose deterministic time history is given. The effect of the type of the target structural response on convergence of the actuator force signal and the error magnitude is investigated.

2. Force of actuator

The state space form equation of a structure excited by wind load f and the shaker-generated force u of size r is as follows.

$$\begin{aligned} \dot{z} &= Az + B_f f + B_u u \\ y &= Cz + D_f f + D_u u \end{aligned} \tag{1}$$

where z is the state vector and y is the output vector of size m. The transfer function of output to input f or u is given by

$$T_{yf} = \frac{Y_f(s)}{F(s)} = C(sI-A)^{-1}B_f \quad \text{or} \quad T_{yu} = \frac{Y_u(s)}{U(s)} = C(sI-A)^{-1}B_u \tag{2}$$

where the scalar s is a complex variable $j\omega$. The inverse of T_{yu} exists only if r equals to m, and the Laplace transform of u providing an identical output to the wind-induced output is determined as

$$U(s) = T_{yu}^{-1}Y_u(s) = T_{yu}^{-1}Y_f(s) = T_{yu}^{-1}T_{yf}F(s) \tag{3}$$

when r is smaller than m, the number of structural responses which can be modulated by u is restricted to r and target structural response should be selected. The Laplace transform of the input realizing the target response $\bar{y}$ of size r is

$$\hat{U}(s) = \hat{T}_{yu}^{-1}\hat{Y}_u(s) = \hat{T}_{yu}^{-1}\hat{Y}_f(s) = \hat{T}_{yu}^{-1}\hat{Y}_{yf}F(s) \tag{4}$$

where $\hat{T}_{yu}^{-1}$ is a sub-matrix of T_{yu}^{-1}. $\hat{T}_{yu}^{-1}$ is constructed by extracting the columns in T_{yu}^{-1} corresponding to the target response.

3. Filter and envelop function

The transfer function of the structural response may have frequency ranges in which the magnitude is as small as zero, and in those ranges, the magnitude of the inverse transfer function increases infinitely. Because the input force is calculated by the product of the inverse transfer function and the output signal, a significant input force may be calculated for the realization of a small magnitude of output components corresponding to the ranges. This implies that the shaking system becomes very sensitive to slight frequency variations of the output signal resulting from measurement noise and spectral leakage, which are inevitable in signal processing using discrete Fourier transform; unnecessarily large input energy excites unexpected frequency responses such that the target response may not be induced. Particularly, a low frequency component leads to a large stroke of the shaker. In this study, the following band-stop filter (BSF) using a cosine function is used to prevent the occurrence of unexpected frequency responses.

$$\hat{U}_p(\omega) = G(\omega)\cdot\hat{U}(s) \tag{5}$$

where

$$G(\omega) = \frac{1-a_{co}}{2}\cos\left(\frac{2\pi}{\omega_2-\omega_1}\omega\right)+\frac{1+a_{co}}{2} \tag{6}$$

$$a_{co} = \begin{cases} \omega<\omega_1; & 1 \\ \omega_1\le\omega\le\omega_2; & 0 \\ \omega>\omega_2; & 1 \end{cases} \tag{7}$$

where, ω_1 and ω_2 are the frequencies defining the cut-off frequency range, and a_{co} is the gain value of the cut-off frequency. Fig. 2(a) shows the shape of the BSF.

In discrete Fourier transform dealing with the finite duration discrete signal as an infinite one multiplied by a rectangular window, the original signal in the time domain is distorted especially in the initial and final time intervals. These distortions can be reduced by using an envelop function so that the given deterministic wind load has ascending and descending time intervals. Although the envelope function changes the deterministic wind load, the effect of this another distortion would be trivial in evaluating the characteristics of a wind-induced response because the more important concern is generally with the intermediate time of the total loading duration when the peak response is expected to occur. Fig. 2(b) shows the shape of the envelope function used in this study.

4. Numerical example

4.1. 76 story wind-induced benchmark building

The wind-induced response simulating actuator is applied to a 76-story 306 meters office tower benchmark building, which is slender with a height-to-width ratio of 306.1/42 = 7.3. Because the

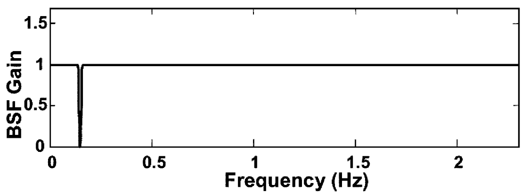

(a) The shape of the band-stop filter

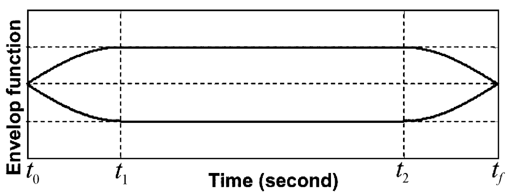

(b) The shape of the envelop function

Fig. 2 Exciter gain shape of the band-stop filter and the envelop function

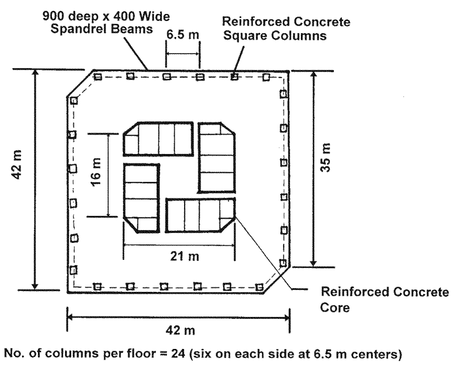

(a) Plan View of the 76-Story Building

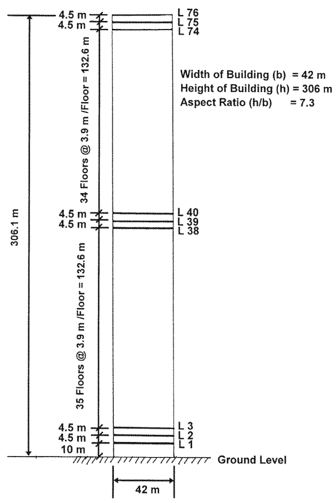

(b) Elevation View of the Building.

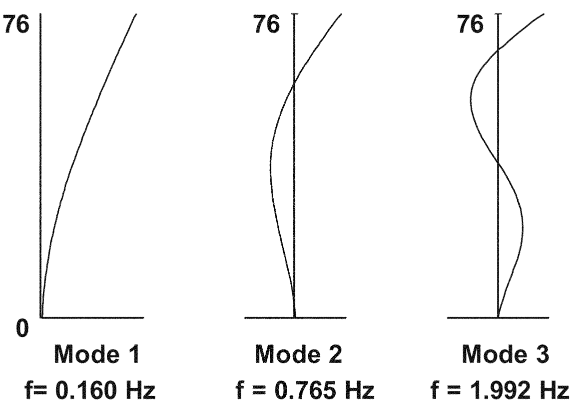

(c) Mode shapes of First Three Modes of the Building.

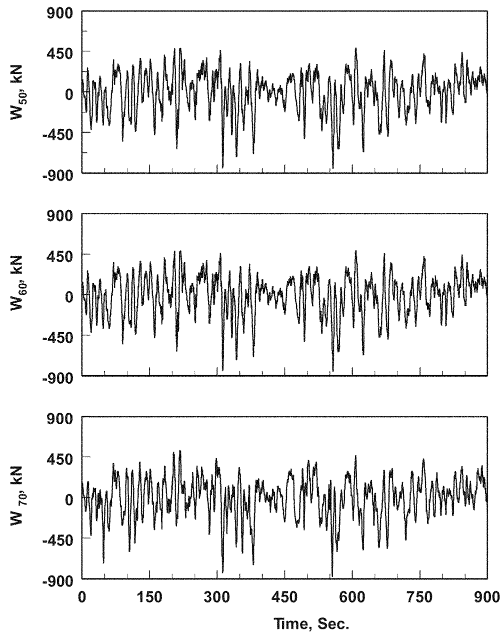

(d) Time Histories of Wind Load on Floors 50, 60 and 70; W_{50}, W_{60} and W_{70}.

Fig. 3 76^{th} story benchmark building model and wind load(Yang, *et al*. 1999)

deterministic across-wind load data are given by wind tunnel tests for this benchmark building, the force of the actuator force realizing the target across-wind induced structural response can be calculated using Eq. (4). In order to reduce the numerical computation time, a 23 degree of freedom (DOF) state reduced-order system model proposed by Yang *et al.* (1999) is used in this study. The wind load vector is modeled physically by lumping wind forces on adjacent floors at the locations that correspond to the 23 DOF model. Figs. 3(a), (b) show the plan view and elevation view of the 76^{th} benchmark building and Figs. 3(c), (d) show the mode shapes of the first three modes of the structure and the time histories of the wind-load.

4.2. Error evaluation criteria

In order to verify the effectiveness of proposed method through comparison between the wind- and actuator-induced structural responses, two error criteria are considered in time and frequency domains, respectively.

In the time domain, the normalized tracking error is defined as

$$e_t = \sqrt{\frac{1}{n}\sum_{i=0}^{n-1}\{x_a(i\Delta t) - x_f(i\Delta t)\}^2 / \max\{|x_f|\}} \tag{8}$$

where Δt denotes time interval, n denotes the data number. $x_a(i\Delta t)$ and $x_f(i\Delta t)$ are, respectively, actuator- and wind-induced structural responses at the ith time step.

In the frequency domain, the normalized tracking error is defined as

$$e_f = \sqrt{\frac{1}{N}\sum_{i=1}^{N}|X_a(\omega_i) - X_f(\omega_i)|^2 / \max\{|X_f|\}} \tag{9}$$

where N is the number of frequency response data, and $X_a(\omega_i)$ and $X_f(\omega_i)$ are the discrete-Fourier transformations of $\ddot{x}_a(t)$ and $\ddot{x}_f(t)$, respectively, at the ith frequency step in the frequency domain.

4.3. LMS excitation

In this section, a LMS which can produce an arbitrary desired force is used as an actuator. LMS is assumed to have mass of 500 metric tons and be installed at 76th floor. The mass is identical to that of an ATMD used as a vibration dissipation device for the benchmark problem. The mass is about 45% of the top floor mass, which is 0.327% of the total mass of the building.

Figs. 4(a) and (b) show the transfer function of the 75th floor acceleration and displacement responses to the force by LMS, and Fig. 4(c) and (d) shows the frequency response functions of excitation forces. It is observed that the acceleration transfer function in Fig. 4(a) has zero at the slightly

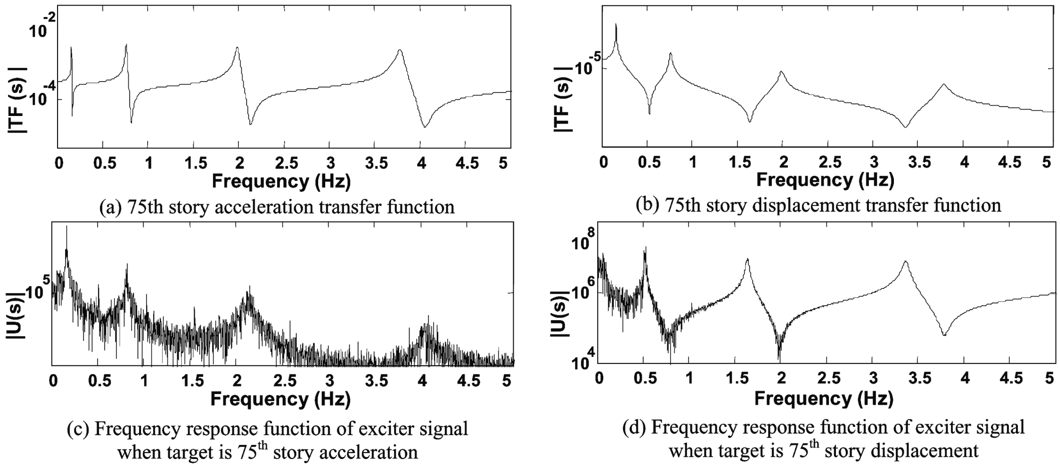

(a) 75th story acceleration transfer function

(b) 75th story displacement transfer function

(c) Frequency response function of exciter signal when target is 75th story acceleration

(d) Frequency response function of exciter signal when target is 75th story displacement

Fig. 4 Transfer function of 75th story responses to LMS

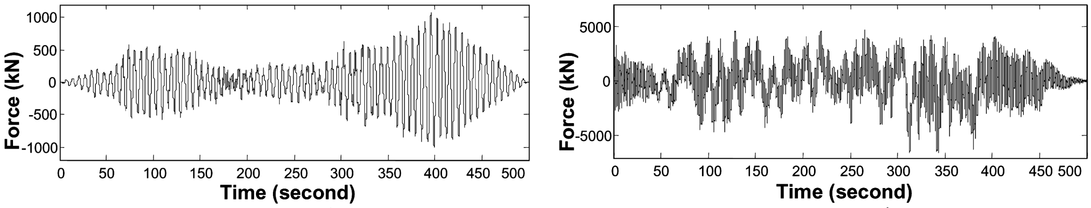

(a) LMS force targeting on 75th floor acceleration (b) LMS force targeting on 75th floor displacement

Fig. 5 LMS force (without BSF)

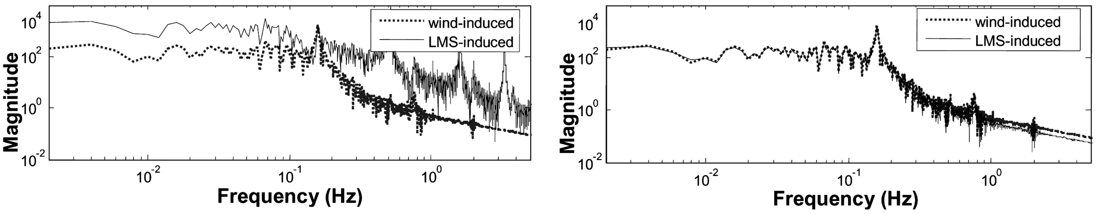

(a) Acceleration response (b) Displacement response

Fig. 6 Frequency response of 75th floor with LMS force targeting displacement response

larger frequency than the first modal frequency whose response is expected to dominate the overall wind induced structural responses.

Fig. 5 shows the frequency response function and the time history of the actuator force obtained without using a filter when the target response is the acceleration or displacement of the 75th floor. A much larger force is required for the shaker to achieve the target displacement than the target acceleration response, and furthermore, the high frequency components shown in Fig. 4(d) result in high speed-switching of the control force, as shown in Fig. 5(b). This undesirable chattering problem causes spillover instability in higher modes by the actuators.

Fig. 6 shows the comparison between the frequency responses of wind- and LMS-induced 75th floor acceleration and displacement when the target response is the 75th displacement. The wind- and LMS-induced displacements coincide well with each other whereas the acceleration responses are very different. Considering that the results shown in Fig. 5 and Fig. 6, and that the magnitude of acceleration response concerned with the serviceability criterion is more important for such high-rise buildings excited by wind load as this benchmark building than displacement response, only acceleration response is considered as the target response for calculating the LMS force from now on.

Numerical analyses are conducted with/without using the BSF and envelop function for different target responses. Table 1 lists the cut-off frequencies used for cancelling previously mentioned undesirable amplification effect due to the zero in the inverse transfer function of each target response. An envelop function with $t_1 - t_0 = 100$ seconds and $t_f - t_2 = 100$ seconds is applied.

Table 1 Cutoff frequency for filter design

Target response	ω_1 (rad/sec)	ω_2 (rad/sec)
75th floor acceleration	1.01	1.13
50th floor acceleration	8.17	8.80
30th floor acceleration	17.59	20.73

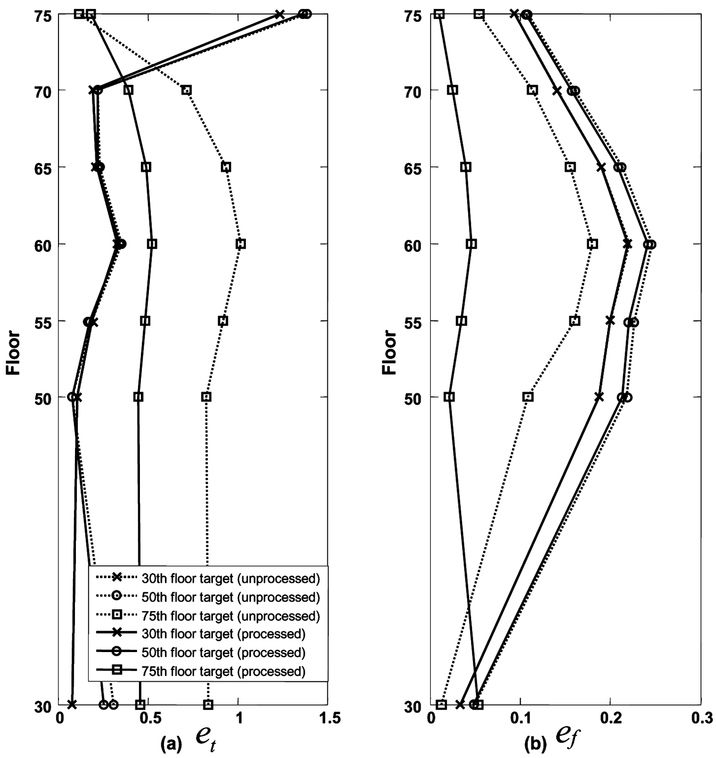

Fig. 7 Error distribution according to the filter usage and target acceleration floor

Fig. 7 shows the floor distribution of the time and frequency domain errors defined in the previous section. The processed signal in the legend of Fig. 7 denotes errors yielded with the BSF. Fig. 7 shows that the processed signal significantly reduces the magnitude of the tracking error when the target response is the 75-floor acceleration, whose transfer function has zero in the vicinity of the first modal frequency (as observed in Fig. 4(a)), but the effect becomes trivial when the target response is the 30th or 50th floor acceleration. Also, the error distribution shows that the targeted responses are almost identical to the wind-induced ones with small magnitude of error while the other non-targeted responses are slightly different from responses. Especially, targeting the 30th or 50th floor acceleration provides greater discrepancy between the wind- and LMS-induced 75-floor accelerations.

The comparison between the results in Fig. 7(a) and (b) indicates that the distribution tendencies of e_t and e_f are quite different. When the targeted response is the 75th floor acceleration, both values of e_t and e_f are the smallest for the corresponding targeted 75th floor acceleration, but the value of e_t becomes larger for the other story responses while the value of e_f is generally the smallest only except for the 30th story acceleration. The larger value of e_t results from the phase difference between the wind- and LMS-induced responses since e_t is calculated by the response difference at the same time step. Because the phase of the wind- induced response is not an important parameter in evaluating the wind resistance performance of a building structure, e_f can be considered as a more appropriate index for evaluating the wind response reproducing performance of LMS than e_t.

Figs. 8 and 9 compare the time histories of the wind- and LMS-induced structural responses for the cases in which the target responses are, respectively, the 75th and 30th floor accelerations and the

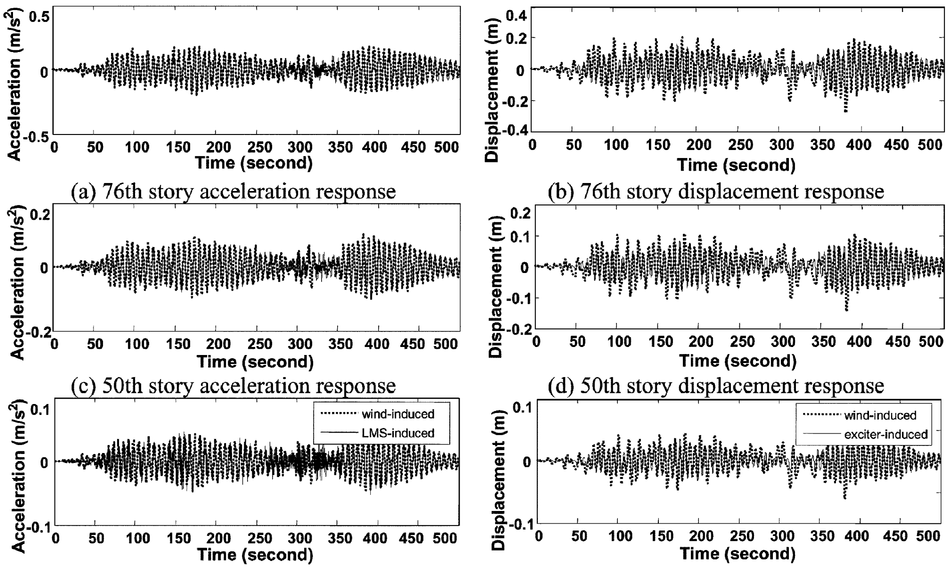

(a) 76th story acceleration response (b) 76th story displacement response
(c) 50th story acceleration response (d) 50th story displacement response
(e) 30th story acceleration response (f) 30th story displacement response

Fig. 8 Wind- and LMS- induced acceleration responses (when the target is 75th floor acceleration)

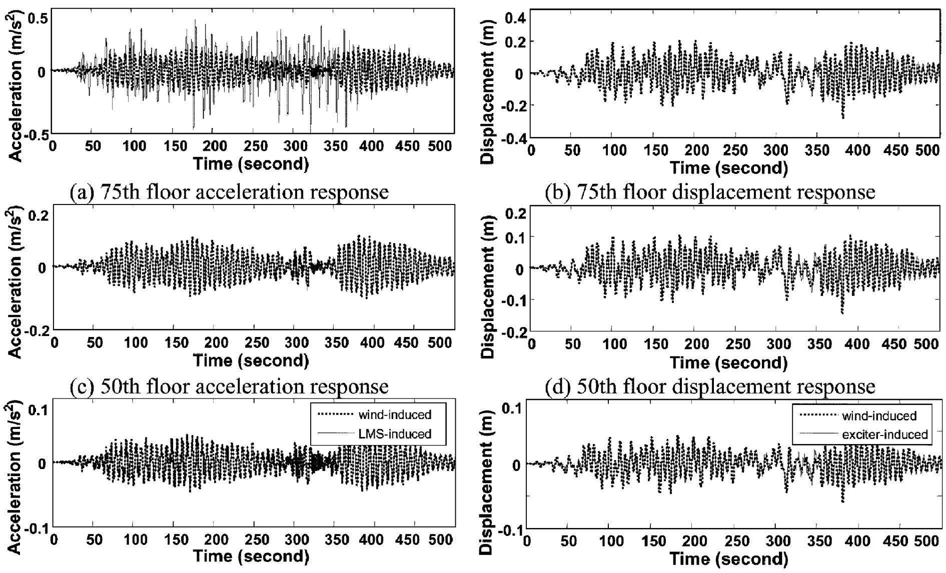

(a) 75th floor acceleration response (b) 75th floor displacement response
(c) 50th floor acceleration response (d) 50th floor displacement response
(e) 30th floor acceleration response (f) 30th floor displacement response

Fig. 9 Wind- and LMS-induced acceleration responses (when the target is 30th floor acceleration)

filter is applied for the design of LMS. Fig. 8 shows that the LMS-induced acceleration responses including the targeted 75th floor acceleration agree well with the wind-induced ones; but displacement responses at all floors are underestimated by LMS. Fig. 9 shows that the shaker simulated the targeted 30th floor acceleration as well as displacement responses but overestimated the 75th floor acceleration.

4.4. ATMD excitation

In the 76th story building benchmark problem, ATMD is used as an example controller, which is composed of a spring, a viscous damper, and the actuator of the LMS. In this section, the ATMD is considered as another exciter. The mass of the ATMD is 500 metric tons, and the undamped natural frequency and damping ratio are 0.16 Hz and 20%, respectively (Yang 1999). The control environments have been simplified; in particular, the actuator dynamics and the controller-structure interaction are not considered in the benchmark problem.

The equation of motion of the building equipped with an ATMD on the top floor can be expressed as

$$\mathbf{M}\ddot{\mathbf{x}} + \mathbf{C}\dot{\mathbf{x}} + \mathbf{K}\mathbf{x} + \mathbf{H}u = \eta\mathbf{W} \tag{10}$$

and considering no wind-load input, the equation of motion of the building can be expressed as

$$\begin{bmatrix} \mathbf{M}_s & 0 \\ \mathbf{0} & m_t \end{bmatrix} \begin{Bmatrix} \ddot{\mathbf{x}}_s \\ \ddot{x}_t \end{Bmatrix} + \begin{bmatrix} \mathbf{C}_s + c_t\mathbf{B}_t\mathbf{B}_t^T & -c_t\mathbf{B}_t \\ -c_t\mathbf{B}_t^T & c_t \end{bmatrix} \begin{Bmatrix} \dot{\mathbf{x}}_s \\ \dot{x}_t \end{Bmatrix} + \begin{bmatrix} \mathbf{K}_s + k_t\mathbf{B}_t\mathbf{B}_t^T & -k_t\mathbf{B}_t \\ -k_t\mathbf{B}_t^T & k_t \end{bmatrix} \begin{Bmatrix} \mathbf{x}_s \\ x_t \end{Bmatrix} = \begin{bmatrix} -\mathbf{B}_t \\ 1 \end{bmatrix} u \tag{11}$$

where, $\mathbf{B}_t$ is the position vector of the ATMD, $\mathbf{M}_s$, $\mathbf{C}_s$ and $\mathbf{K}_s$ are the mass, damping coefficient and stiffness matrix of the structure and m_t, c_t and k_t are the mass, damping coefficient and stiffness of the ATMD, respectively.

Fig. 10(a) shows the transfer function between the 75th floor acceleration and the absolute acceleration of the ATMD. Zero point is not observed in the vicinity of the first modal frequency unlike the case for LMS, which indicates that the BSF is not required to prevent the ATMD from exciting the unexpected frequency responses. Fig. 10(b) shows the frequency response of the actuator force of the ATMD, and Fig. 10(c) and (d) show the frequency and time responses of the effective force applied to the structure by the ATMD.

Fig. 11 shows the time history comparison between the wind-induced acceleration and the ATMD-induced one for the target of the 75th story acceleration response. All acceleration responses coincide well with each other, but the displacement response shows slight underestimation and overestimation according to the time ranges.

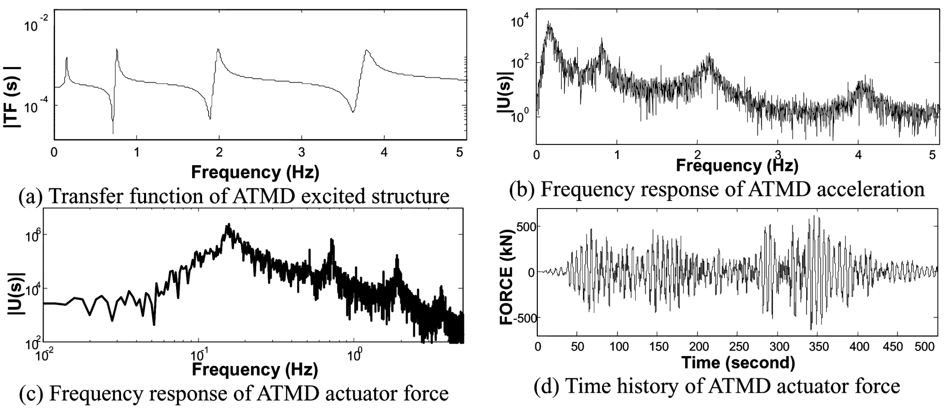

(a) Transfer function of ATMD excited structure
(b) Frequency response of ATMD acceleration
(c) Frequency response of ATMD actuator force
(d) Time history of ATMD actuator force

Fig. 10 ATMD Excitation

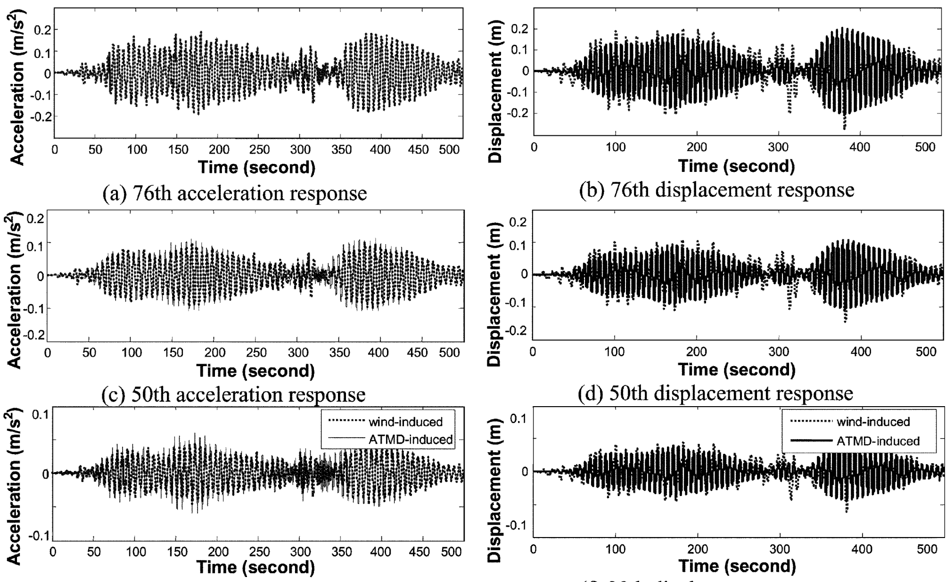

(a) 76th acceleration response
(b) 76th displacement response
(c) 50th acceleration response
(d) 50th displacement response
(e) 30th acceleration response
(f) 30th displacement response

Fig. 11 Wind and ATMD-induced acceleration responses (when the target is 75th floor acceleration)

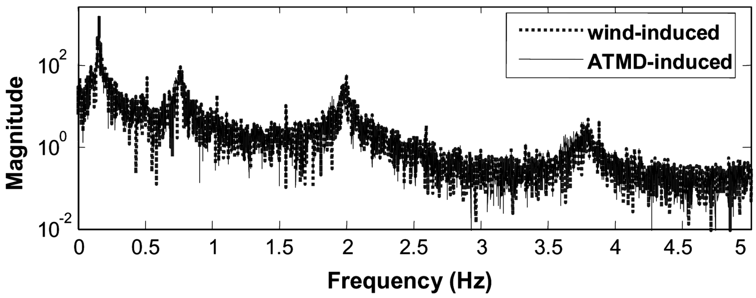

Fig. 12 Frequency response of wind and ATMD induced 75th floor accelerations

Fig. 12 shows the comparison between the frequency responses of the 75th floor acceleration. The wind- and the ATMD-induced responses show good agreement over all frequency ranges.

Fig. 13 shows the error distribution according to the floor of the targeted acceleration response. From Fig. 13(b), which shows the smallest value of e_f over all the floors when the target response is the 75th floor acceleration, ATMD targeting the 75th floor acceleration can be considered to provide the best performance, and it can exactly reproduce the wind-induced acceleration response of all floors including the targeted 75th floor.

4.5. Comparison between LMS and ATMD

Fig. 14 shows the time history of the actuator forces in LMS and ATMD excitation systems. The peak actuator force required for ATMD is larger than that for LMS. Fig. 15 compares the stroke of LMS with/without filter and ATMD. The stroke of LMS with filter is much smaller than that of LMS without filter or ATMD. This fact implies that ATMD requires a large stroke to show good performance for the

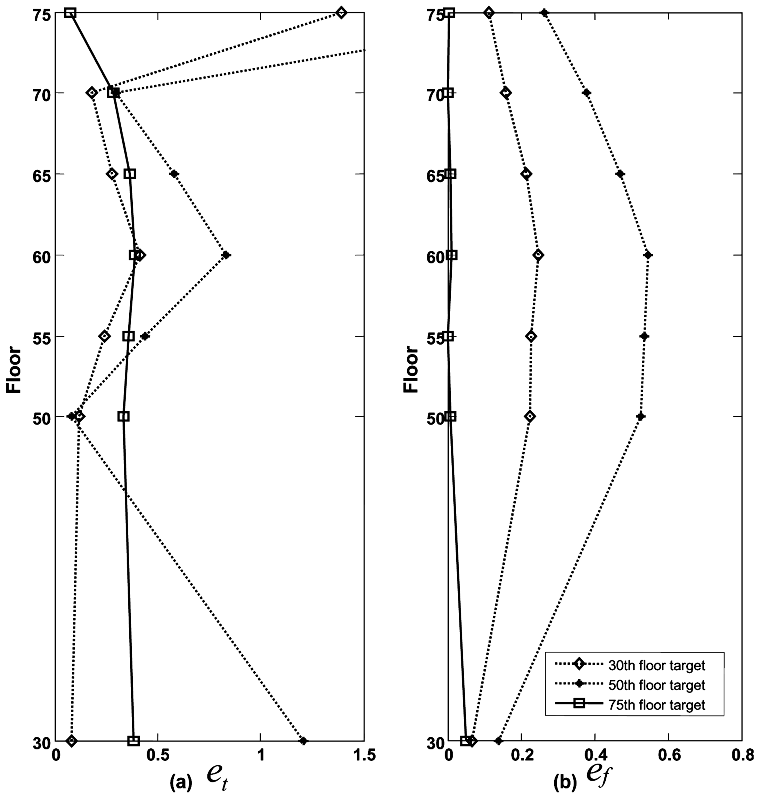

Fig. 13 Error distribution with ATMD excitation

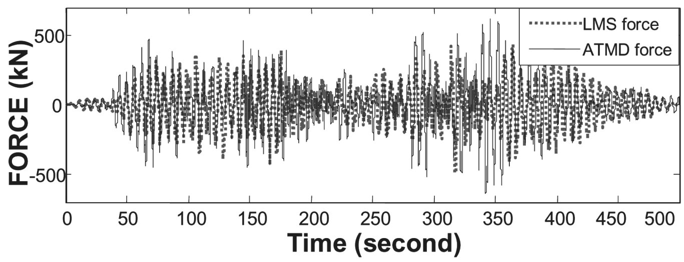

Fig. 14 Comparison between actuator forces in LMS and ATMD

realization of the wind-induced response, and this stroke requirement should be checked in the design of ATMD.

Table 2 shows the numerical values of the error, actuator force, and actuator stroke in LMS with/without filter, and ATMD systems. The errors are obtained when the target and evaluation responses are identical, and the actuator force and stroke are obtained when the target response is the 75th floor acceleration. The facts observed from Figs. 14 and 15 reveal that the performance of LMS can be enhanced by using a BSF and that ATMD reproduces wind-induced responses better than LMS but that ATMD requires a larger actuator force and stroke than LMS.

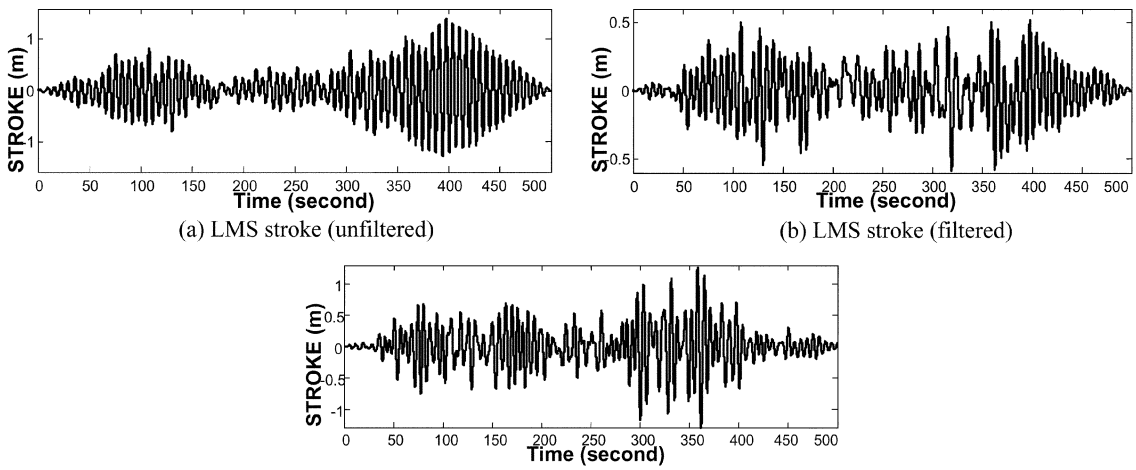

(a) LMS stroke (unfiltered) (b) LMS stroke (filtered)

(c) ATMD stroke

Fig. 15 Stroke comparison

Table 2 Comparison between LMS and ATMD

		LMS (unfiltered)	LMS (filtered)	ATMD
75th floor acceleration	e_t	0.117	0.192	0.074
	e_f	0.054	0.011	0.003
50th floor acceleration	e_t	0.081	0.081	0.083
	e_f	0.219	0.213	0.525
30th floor acceleration	e_t	0.082	0.082	0.082
	e_f	0.034	0.033	0.065
Stroke	Peak (m)	1.402	0.519	1.265
	RMS (m)	0.436	0.183	0.333
Actuator force	Peak (kN)	1068.22	441.68	655.78
	RMS (kN)	323.92	136.44	170.39

5. Conclusions

Design of excitation systems for simulating wind-induced responses of a building structure was presented as a preliminary study for evaluating wind-resistance characteristics of practical building structures. The actuator forces of LMS and ATMD were obtained using the inverse transfer function of structural responses. Also, a band stop filter was used in LMS to prevent undesirable modal excitations, and an envelop function was used to reduce the error occurring in transient initial states in both LMS and ATMD. The numerical analyses results from a 76-story benchmark building confirmed that the structural responses of a building structure excited by wind loads acting at all floors could be reproduced by the proposed excitation systems installed at a specific floor. The performances of the excitation systems were dependent on the type and position of the target structural response, the acceleration is more suitable as target responses, because a large and high speed changing control force is required when displacement is used as target response. In order to enhance practical applicability of the proposed wind-response simulating excitation systems, finite element model updating based on measured data, compensating the dynamic characteristics of the excitation systems, and the scaling or restriction of the excitation force or stroke to prevent damage of a practical building and so on should be considered in a further study.

Acknowledgements

Authors express gratitude to the Korea Science and Engineering Foundation (KOSEF) for their support of this work through Smart Infra-Structure Technology Center (SISTeC) at Korea Advanced Institute of Science and Technology (KAIST), and the Ministry of Education & Human Resources Development through the Second Stage of BK21.

References

Alvin, K. F. and Park, K. C. (1994), "Second-order structural identification procedure via state-space-based system identification", *AIAA J.*, **32**, 397-406.

Au, F. T. K., Jiang, R. J. and Cheung, Y. K. (2004), "Parameter identification of vehicles moving on continuous bridges", *J. Sound. Vib.*, **269**, 91-111.

Dyke, S. J., Spencer Jr., B. F., Quast, P., Sain, M. K., Kaspari Jr., D. C. and Soong, T. T. (1994), "Experimental verification of acceleration feedback control strategies for an active tendon system", *Technical Report NCEER-94-0024*, *State University of New York at Buffalo*, Buffalo, NY.

Friswell, M. I. and Mottershead, J. E. (1995), *Finite Element Model Updating in Structural Dynamics*, Kluwer Academic Publishers, Boston, London.

Herman, V. A. and Bart, P. (2003), "Sensors and systems for structural health monitoring", *J. Struct. Cont.*, **10**, 117-125.

Juang, J. N. (1994), *Applied System Identification*, Prentice Hall, Englewood Cliffs, NJ.

Ljung, L. (1987), *System Identification: Theory for the User*, Prentice Hall, Englewood Cliffs, NJ.

Madenci, E. and Barut, A. (1994), "A free-formulation-based flat shell element for non-linear analysis of thin composite structures", *Int. J. Numer. Meth. Eng.*, **37**, 3825-3842.

Yang, J. N., Agrawal, A. K., Samali, B. and Wu, J. C. (1999), "A benchmark problem for response control of wind-excited tall buildings", *World Wide Website*, *http://www.eng.uci.edu/~jnyang/benchmark.htm*.

Yu, E., Whang, D. H., Conte, J. P., Stewart, J. P. and Wallace, J. W. (2005), "Forced vibration testing of buildings using the linear shaker seismic simulation (LSSS) testing method", *Earthq. Eng. Struct. Dyn.*, **34**, 737-761.

CC